

Electronic Supplementary Information

Self-Supported N-Doped CNT Arrays for Flexible Zn-Air Batteries

Lina Liu,^a Xiao Zhang,^b Feng Yan,^b Bo Geng,^a Chunling Zhu,^{*a} and Yujin Chen^{*abc}

^a Key Laboratory of Superlight Materials and Surface Technology, Ministry of Education,
College of Material Sciences and Chemical Engineering, Harbin Engineering University, Harbin
150001, China

^b College of Physics and Optoelectronic Engineering, Harbin Engineering University, Harbin
150001, China

^c School of Materials Science and Engineering, Zhengzhou University, Zhengzhou 450001,
China

*E-mail: zhuchunling@hrbeu.edu.cn; chen yujin@hrbeu.edu.cn

Experimental Section

Materials and Reagents: Cobalt nitrate hexahydrate, ferric nitrate nonahydrate and iron chloride hexahydrate was purchased from Sinopharm Chemical Reagent Co., Ltd. PVA-1788 powder were purchased from Aladdin Industrial Corporation. Urea, Ammonium fluoride and dicyandiamide were purchased from Tianjin Guangfu Fine Chemical Research Institute. Zinc acetate dihydrate and potassium hydroxide were purchased from Xilong Scientific Co., Ltd. Ethanol was purchased from Tianjin Fuyu Fine Chemical Co., Ltd. It is worth noting that, all chemicals were used without any further treatment, and all aqueous solutions were prepared using ultrapure water.

Synthesis of Electrocatalysts:

Preparation of CoFe nanowire (NWs)/CFC: Before growth of CoFe NWs, the CFC substrates were first cleaned by sonication in 10 wt% KMnO_4 solution for 10 min, then sonication was continued in deionized (DI) water and ethanol in turn until the solution was clear, finally the cleaned CFC was dried in oven. The preparation of CoFe NWs was refer to a previous method.^[S1] In a typical process, 0.388 g (1.33 mmol) of $\text{Co}(\text{NO}_3)_2 \cdot 6\text{H}_2\text{O}$, 0.27 g (0.66 mmol) of $\text{Fe}(\text{NO}_3)_3 \cdot 9\text{H}_2\text{O}$, 0.186 g (5 mmol) of NH_4F and 0.6 g (10 mmol) of urea were dissolved successively in 40 mL DI water under stirring. After stirring 10 min at room temperature, the solution was quickly poured into the autoclave, and a piece of above cleaned CFC substrate ($3 \times 4 \text{ cm}^2$) was immersed in the admixture solution. Keep at 120°C still for 6 h in the oven to synthesize the CoFe NWs arrays grown on CFC. After then, the CoFe NWs/CFC

was taken out, and washed successively with water and ethanol, and then dried at 40°C in vacuum dried overnight. The mass loading of the CoFe NWs on the CFC is 1.5 mg cm⁻².

Preparation of Co NWs/CFC: For reference, Co NWs/CFC was also prepared using the same method to the preparation of CoFe NWs/CFC precursor, except for the adding of Fe(NO₃)₃·9H₂O. Because of the absence of Fe(NO₃)₃·9H₂O, the addition amount of Co(NO₃)₂·6H₂O was increased to 0.582 g (2 mmol). The mass loading of the Co NWs is about 2.5 mg cm⁻².

Preparation of FeOOH nanorod (NRs)/CFC: FeOOH NRs/CFC was synthesized for comparison.^[S2] In details, 0.4 g FeCl₃·6H₂O and 0.24 g Na₂SO₄ were dissolved successively in 35 mL DI water, the solution was transfer to the 50 mL autoclave after stirring for 10 min. Keeping at 120°C for 6 h in the oven to synthesize FeOOH NRs/CFC. The mass loading of the FeOOH NRs on the CFC is 1.5 mg cm⁻².

Preparation of CoFe@NCNT/CFC: CoFe@NCNT/CFC was obtained by a simple one-step pyrolysis method. In a typical process, a piece of the as-prepared CoFe NWs/CFC (3 × 4 cm²) and 1.5 g of dicyandiamide (DCDA) were placed in two separate ceramic boats in furnace, which the DCDA was located at the upstream side of the argon atmosphere. The samples and DCDA were first thermally annealed at 400°C for 2 h under flowing Ar gas with a heating ramp rate of 5 °C min⁻¹. Then the temperature was further raised to 800°C, and maintained at this temperatures for another 2 h. After carbonization, the CoFe Nws arrays were turned into CoFe alloy NPs embedded N-doped carbon nanotube arrays and marked as CoFe@NCNT/CFC. The mass loading of CoFe@NCNTs on carbon cloth was calculated to be 1.2 mg cm⁻². For reference,

the Co@NCNT/CFC and Fe@NCNT/CFC were also fabricated using Co NWs /CFC and FeOOH NRs/CFC as precursor, and carbonized under the same condition of the CoFe@NCNT/CFC. The mass loading of the Co@NCNTs on CFC is determined to be 2 mg cm⁻² by weighting the CFC substrate before and after growth of the NCNT arrays, larger than that of CoFe@NCNTs/CFC (1.2 mg cm⁻²) and Fe@NCNTs/CFC (1 mg cm⁻²). In order to investigate the effect of the atomic ratio of Co/Fe in the electrocatalytic performance of final products, the precursor nanowires with different molar ratio of addition amount of Co/Fe (Co:Fe = 3:1, 2:1, 1:1, 1:2 at molar ratio) were prepared, and carbonized at 800°C, the corresponding products were denoted as CoFe_{3:1}@NCNT/CFC, CoFe_{2:1}@NCNT/CFC, CoFe_{1:1}@NCNT/CFC and CoFe_{1:2}@NCNT/CFC respectively. In addition, the effect of carbonization temperature was also investigated through change the pyrolysis temperature (700°C, 800°C, and 900°C) of CoFe NWs/CFC (Co:Fe = 2:1) precursor. For a comparison, the commercial 20 wt% Pt/C and IrO₂ catalyst coated carbon cloth were also prepared with the same loading mass to CoFe@NCNTs, respectively.

Materials Characterization: The microscopic morphologies and size of as prepared catalyst and precursor were characterized by field-emission scanning electron microscopy (SEM, Hitachi SU70) and transmission electron microscope equipped with a Gatan imaging filter (GIF) (TEM, FEI Tecnai-F20), and elemental mapping was also obtained from Tecnai-F20 instrument. XRD data was measured by a Rigaku D/max-2600/PC with Cu K α radiation ($\lambda=1.5418\text{\AA}$), and Raman spectroscopy was analyzed using a Raman spectrometer (Lab RAMA ramis, Horiba Jobin Yvon) with a Ne-He laser operated at 488 nm wave length, to further confirm the structures of our

catalyst. X-ray Photoelectron Spectrometer (XPS) analyses were carried out by using a spectrometer with Al K α radiation (hv=1486.6 eV) on a Thermofisher Escalab Xi+. The binding energies were corrected by setting the C1s peak at 284.8eV. The nitrogen adsorption-desorption isotherms and the pore size distributions were measured by a Micromeritics ASAP 2020 surface area analyzer. The specific surface area was calculated using Brunauer-Emmett-Teller (BET) model.

Electrochemical Measurements: The electrochemical activities of our catalysts toward ORR and OER reactions were measured using a standard three-electrode system (CHI 760D, CH Instrument, USA) in 0.1 M KOH solution. The self-supported CoFe@NCNT/CFC catalyst can be used directly as the working electrode, while the carbon rod and Ag/AgCl (KCl saturated) were employed as counter electrode and reference electrode, respectively. For ORR test, the CoFe@NCNT/CFC was directly adhered on the glassy carbon rotating disk electrode by Nafion (1 μ L, 5wt %) to prepare the working electrode. Cyclic voltammograms (CV) measurements were taken at a scan rate of 50 mV s⁻¹ in O₂- and Ar-saturated KOH solution, while the linear sweeping voltammetry (LSV) were performed at a rotating rate ranging from 400 to 2025 rpm with a scan rate of 10 mV s⁻¹. The electron transfer numbers (n) and kinetic current density (J_k) were calculated according to Koutecky-Levich equations:

$$\frac{1}{J} = \frac{1}{J_L} + \frac{1}{J_k} = \frac{1}{B\omega^{\frac{1}{2}}} + \frac{1}{J_k} \quad \text{S-1}$$

$$B = 0.62nFC_0D_0^{\frac{2}{3}}V^{\frac{1}{6}} \quad \text{S-2}$$

where J is the measured current density, J_k and J_L are the kinetic and limiting current densities

respectively, ω is the angular velocity of the disk, n is the electron transfer number, F is the Faraday constant ($96485 \text{ C}\cdot\text{mol}^{-1}$), C_0 is the bulk concentration of O_2 ($1.2 \times 10^{-6} \text{ mol}\cdot\text{cm}^{-3}$), D_0 is the diffusion coefficient of O_2 ($1.9 \times 10^{-5} \text{ cm}^2\cdot\text{s}^{-1}$), and ν is the kinematic viscosity of the electrolyte ($0.01 \text{ cm}^2\cdot\text{s}^{-1}$).^[S3]

Rotating ring-disk electrode (RRDE) measurement was performed to further verify the ORR pathways and estimate the n and production of H_2O_2 . The disk electrode was scanned at a rate of 10 mV s^{-1} and the ring potential was constant at 1.3 V vs. RHE. The hydrogen peroxide yield ($\text{H}_2\text{O}_2 \%$) and transfer number (n) were determined by the followed equations: ^[S4]

$$H_2O_2(\%) = 200 \times \frac{I_R / N}{I_D + I_R / N} \quad \text{S-3}$$

$$n = 4 \times \frac{I_D}{I_D + I_R / N} \quad \text{S-4}$$

Where I_d is disk current, I_r is ring current, and N is current collection efficiency of the Pt ring. N was determined to be 0.40.

The OER activity was evaluated using LSV measurement at a scan rate of 5 mV s^{-1} , and a piece of the CoFe@NCNTs/CFC with a geometrical area of 1.0 cm^2 was directly used as working electrode. The Tafel slopes were obtained from the corresponding LSV curves and calculated basis the following Tafel equation: $\eta = a + b \log |j|$, where η represents the overpotential, j represents cathodic current density, a is the Tafel constant, and b is the Tafel slope. Furthermore, turnover frequency (TOF) data was calculated through a previous method.^[5] The number of active sites (n) was calculated through CV in neutral phosphate buffer at a scan rate of 50 mV s^{-1} . The TOF data of the OER electrocatalysts can be obtained by using the following

equation,

$$\text{TOF}(S^{-1}) = (J \times A) / (4 \times n \times F) \quad \text{S-5}$$

where J is the OER current density, A represents the surface area of the anode, and F is the Faraday constant.

Assembly of liquid rechargeable Zinc-air batteries: Measurements of the liquid Zn-air battery with our catalyst were performed under atmosphere condition using home-made electrochemical cells. A polished zinc plate was used as the anode, and electrolyte was 6 M KOH containing 0.2 M $\text{Zn}(\text{CH}_3\text{COO})_2$ for rechargeable Zn-air batteries. The self-supported CoFe@NCNTs/CFC catalyst attached to gas diffusion layer (YLS-26 Carbon paper) was served as air electrode. Galvanostatic discharge-charge cycling tests were performed using a LAND CT2001A battery test system at 10 mA cm^{-2} and 20 mA cm^{-2} with 10 min per cycle. For comparison, commercial Pt/C+IrO₂ (mass ratio is 1:1) with the same loading mass to CoFe@NCNTs catalyst was used as a reference.

Assembly of flexible solid zinc-air batteries: To the assembled flexible all-solid-state Zn-air battery, a polished zinc plate was used as anode, and a piece of CoFe@NCNTs/CFC catalyst directly used as the air cathodes. The preparation process of solid electrolyte was as follow. First of all, 5 g polyvinyl alcohol (PVA-1788) powder was dissolved in 50.0 mL deionized water of 90°C under stirring. After stirring for 1.5 h, 5.0 mL of 18.0 M KOH containing 0.02 M $\text{Zn}(\text{CH}_3\text{COO})_2$ was added into above mixture, and kept stirring until the electrolyte solution became uniform (about 30 min). Subsequently, the above solution was poured into a square

glass groove to form a thin film (about 1 mm), after being freeze at -10 °C overnight, and then thawed at room temperature. Finally, the flexible air electrode and zinc plate were attached to the two sides of PVA gel (1 × 3 cm), and then two pieces of flexible acrylic tape was used to seal the all-solid-state Zn-air battery. All measurements of the home-made flexible all-solid-state Zn-air batteries were carried out using an electrochemical work-station (CHI 760D, CH Instrument, USA) and a LAND CT2001A multi-channel battery testing system. The time of each charge/discharge cycles is 10 min. Commercial Pt/C+IrO₂ (mass ratio is 1:1) catalyst was used as a reference.

Calibration of RHE electrode: The RHE calibration of Ag/AgCl electrode was performed in H₂-saturated 0.1 M KOH electrolyte. Pt wire was used as a working electrode, and the cyclic voltammetry (CV) curves were run at 1 mV s⁻¹. The average of the two potentials at the current crossed zero was taken to be the thermodynamic potential for the hydrogen electrode reaction. In 0.1 M KOH, $E_{(\text{RHE})} = E_{(\text{Ag}/\text{AgCl})} + 0.969 \text{ V}$.

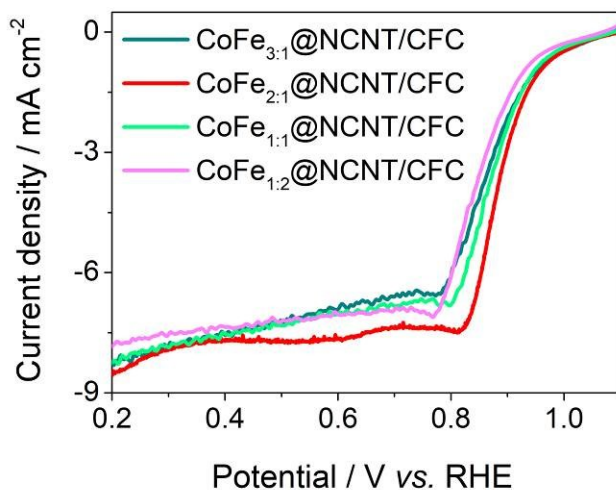


Figure S1. Polarization curves of CoFe@NCNTs/CFC with different content ratio of Co to Fe (Co:Fe = 3:1, 2:1, 1:1, 1:2) towards the ORR in 0.1 M KOH electrolyte. (carbonization temperature: 800°C)

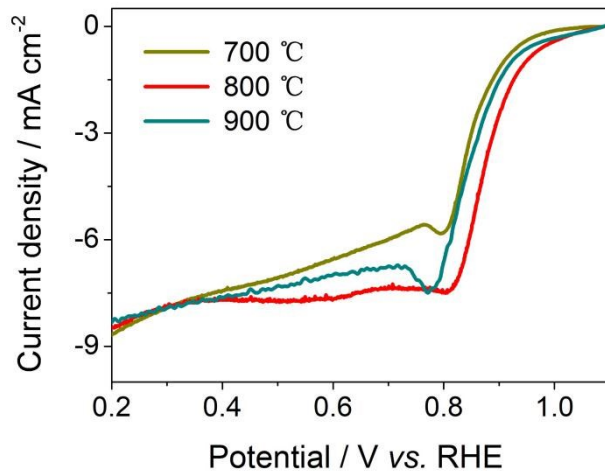


Figure S2. Polarization curves of CoFe@NCNTs/CFC (ratio of Co to Fe is 2:1) obtained at different carbonization temperature (700°C, 800°C, 900°C) towards the ORR in 0.1 M KOH electrolyte.

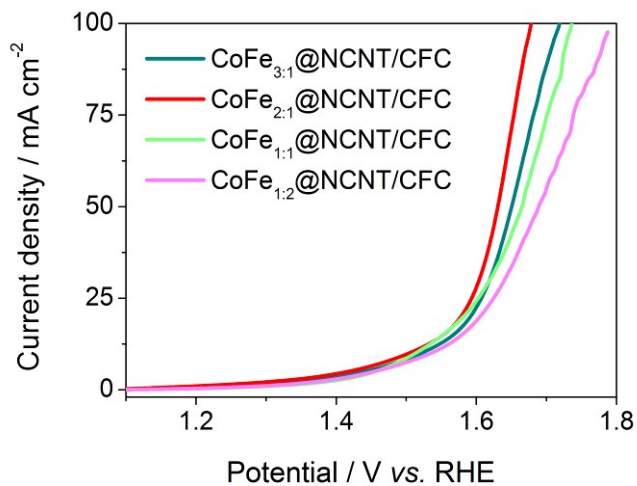


Figure S3. Polarization curves of CoFe@NCNTs/CFC with different content ratio of Co to Fe (Co:Fe = 3:1, 2:1, 1:1, 1:2) towards the OER in 0.1 M KOH electrolyte. (carbonization temperature: 800°C)

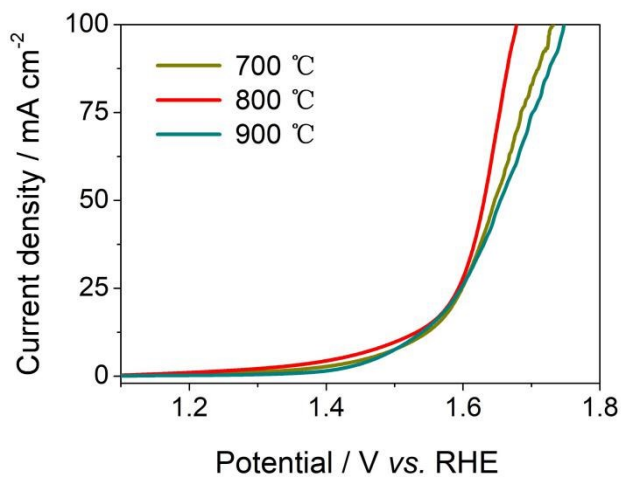


Figure S4. Polarization curves of CoFe@NCNTs/CFC (ratio of Co to Fe is 2:1) obtained at different carbonization temperature (700°C, 800°C, 900°C) towards the OER in 0.1 M KOH electrolyte.

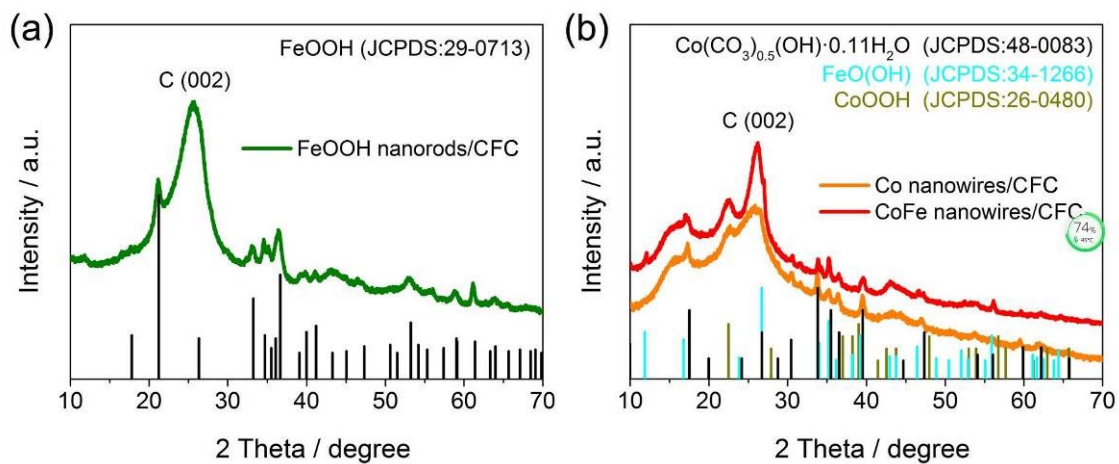


Figure S5. XRD patterns of (a) FeOOH NRs/CFC, (b) Co NWs/CFC and CoFe NWs/CFC.

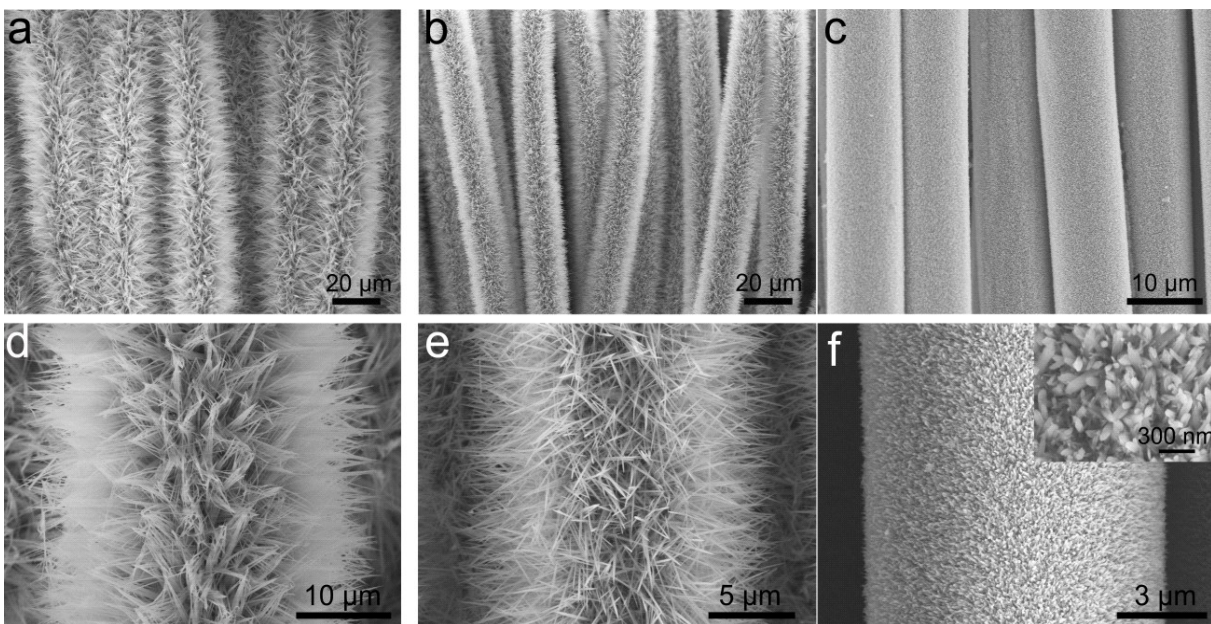


Figure S6. SEM images of (a,d) Co NWs/CFC, (b,e) CoFe NWs/CFC and (c,f) FeOOH NRs/CFC.

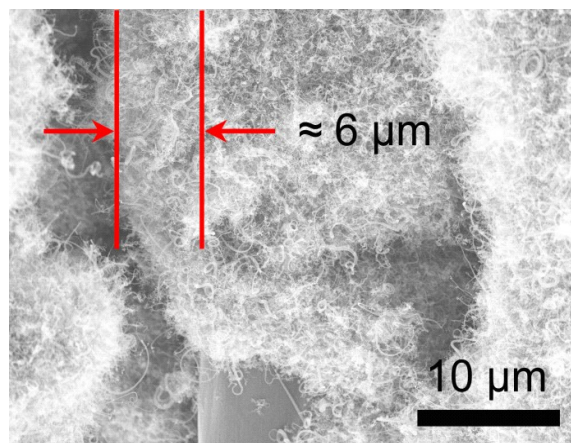


Figure S7. SEM image of the Co@NCNT/CFC.

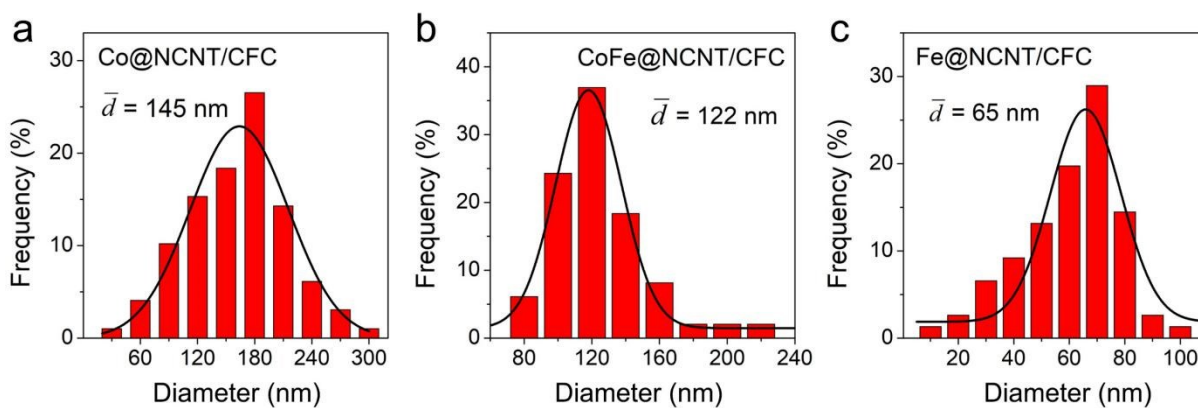


Figure S8. The diameter distribution diagram of the NCNTs of Co@NCNT/CFC, Fe@NCNT/CFC, CoFe@NCNT/CFC self-supported electrode.

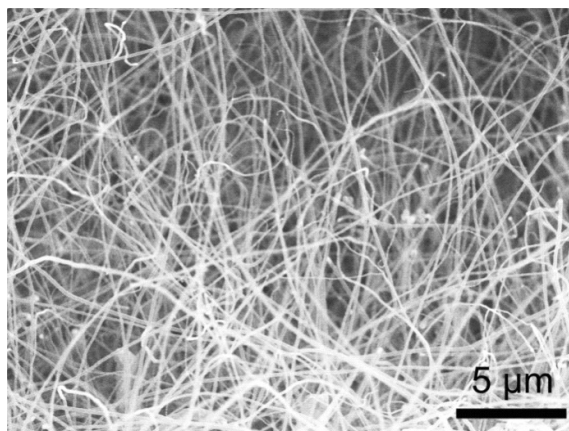


Figure S9. SEM image of CoFe@NCNT/CFC (ratio of Co to Fe is 2:1 at molar ratio and carbonization temperature is 800 °C).

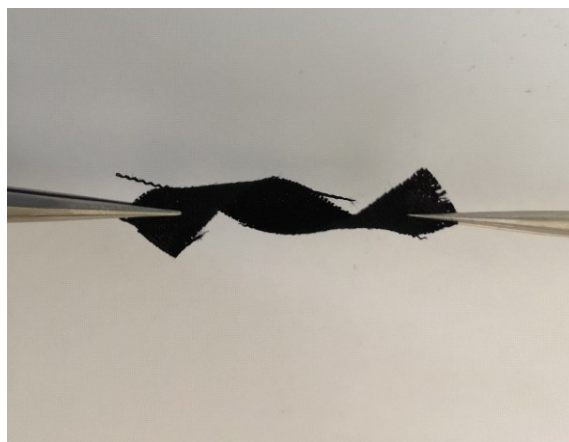


Figure S10. The photograph exhibits the flexibility of the self-supported CoFe@NCNT/CFC electrode.

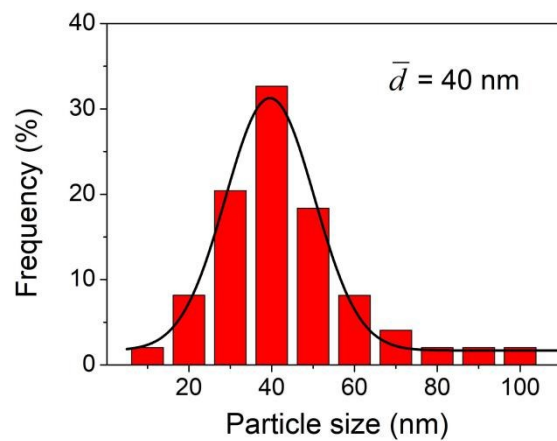


Figure S11. The size distribution diagram of the CoFe particle in CoFe@NCNT/CFC.

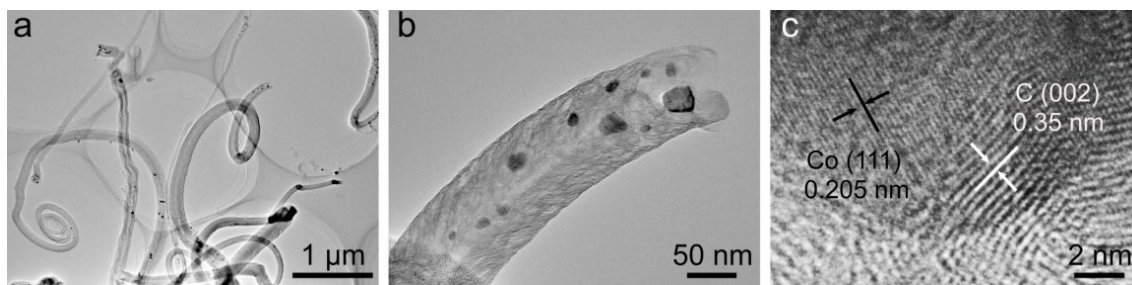


Figure S12. (a,b) TEM and (c) HRTEM images of Co@NCNT/CFC.

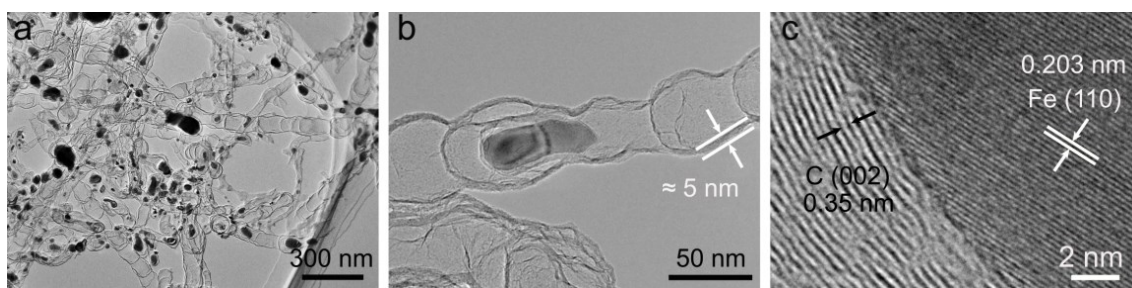


Figure S13. (a,b) TEM and (c) HRTEM images of Fe@NCNT/CFC.

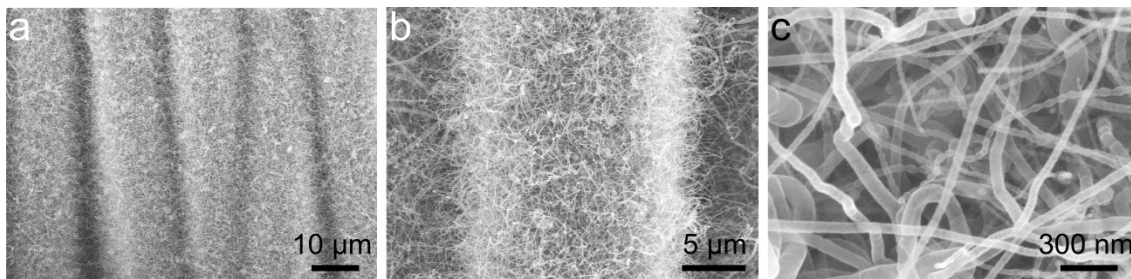


Figure S14. SEM images of CoFe@NCNT/CFC (ratio of Co to Fe is 3:1) carbonized at 800°C.

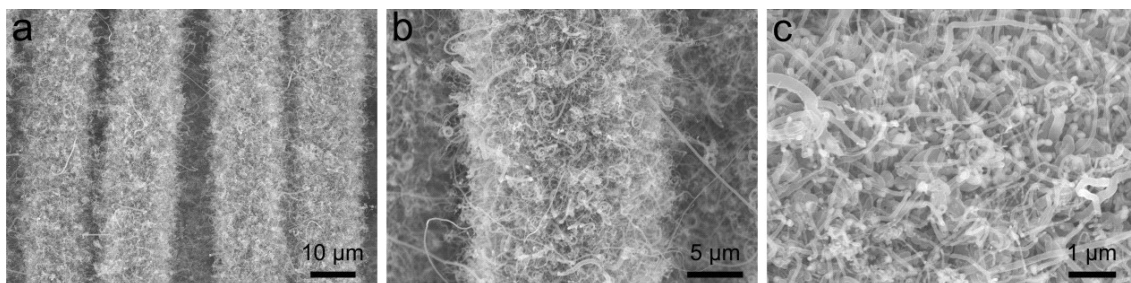


Figure S15. SEM images of CoFe@NCNT/CFC (ratio of Co to Fe is 1:1) carbonized at 800°C.

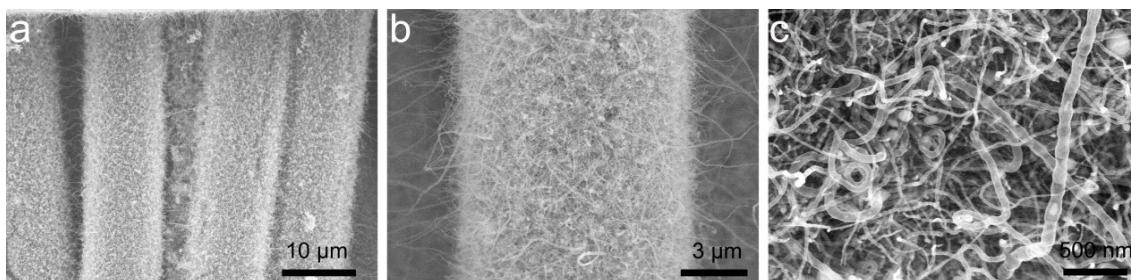


Figure S16. SEM images of CoFe@NCNT/CFC (ratio of Co to Fe is 1:2) carbonized at 800°C.

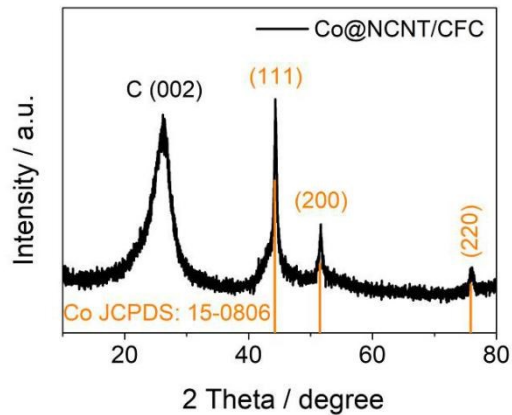


Figure S17. XRD pattern of the Co@NCNT/CFC.

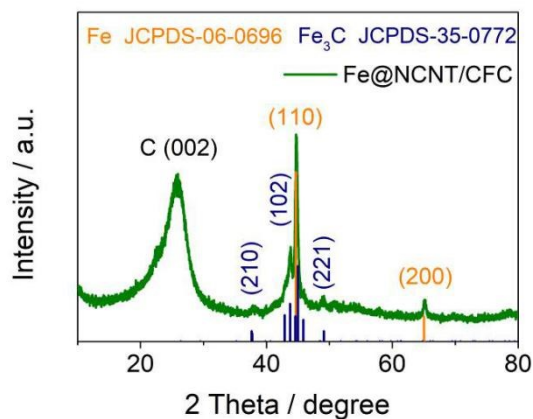


Figure S18. XRD pattern of the Fe@NCNT/CFC.

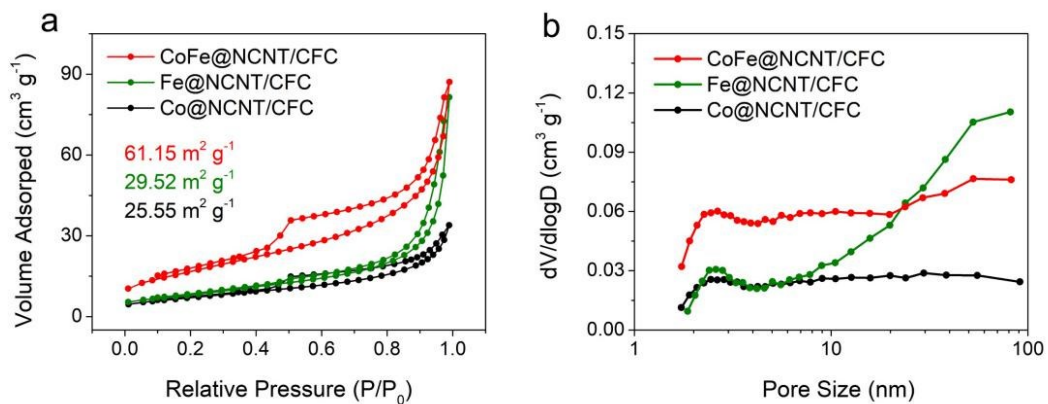


Figure S19. (a) The nitrogen adsorption-desorption isotherms, and (b) pore size distributions of the Co@NCNT/CFC, Fe@NCNT/CFC and CoFe@NCNT/CFC.

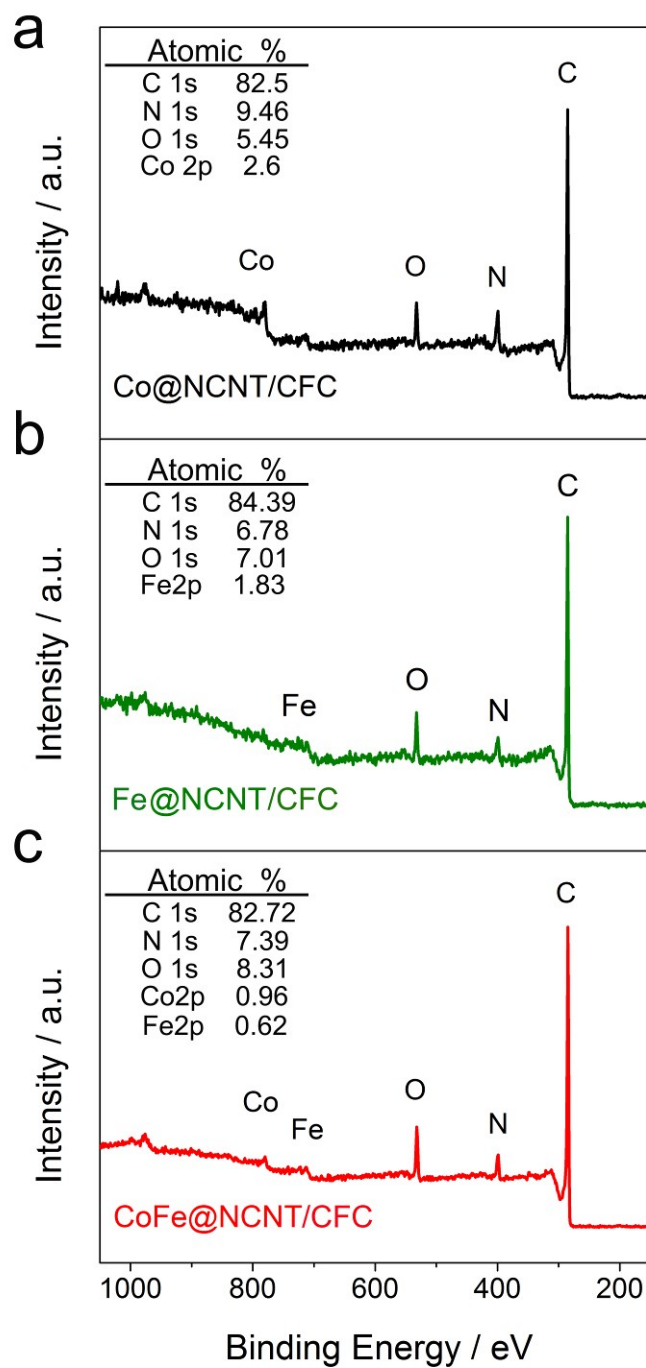


Figure S20. The XPS survey spectrum of (a) Co@NCNT/CFC, (b) Fe@NCNT/CFC and (c) CoFe@NCNT/CFC.

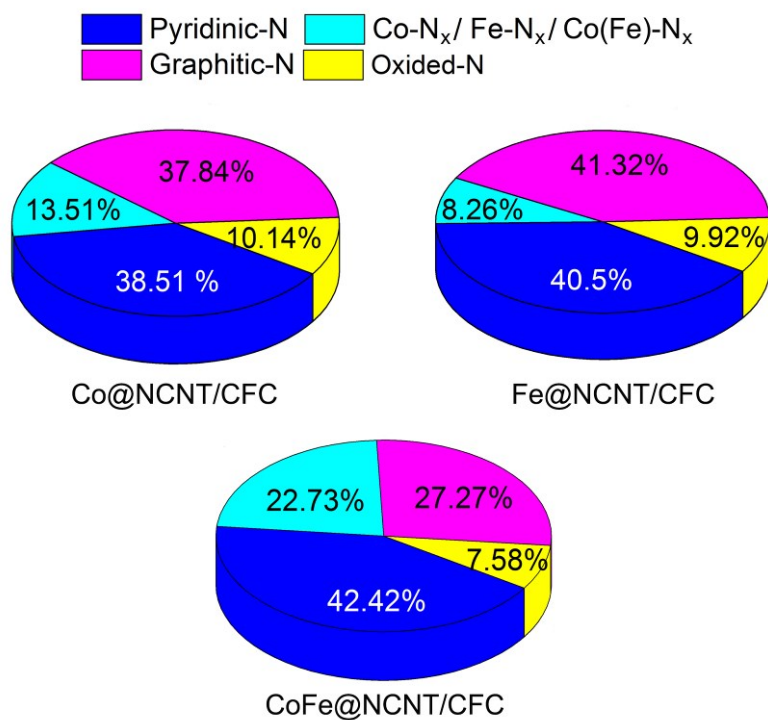


Figure S21. The proportion of various N species of the N element in Co@NCNT/CFC, Fe@NCNT/CFC and CoFe@NCNT/CFC.

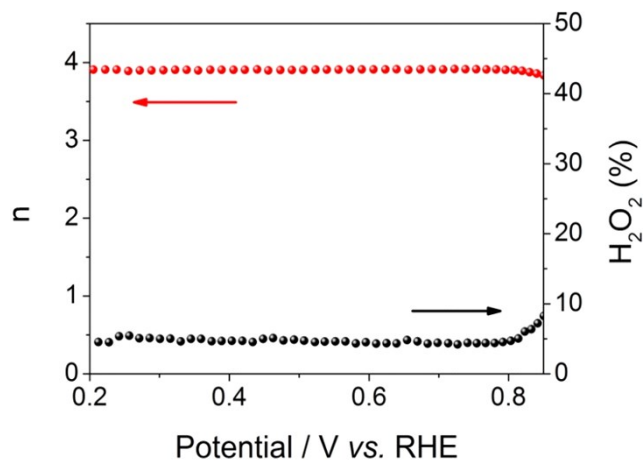


Figure S22. The H₂O₂ yield and electron transfer number (n) of CoFe@NCNT/CFC.

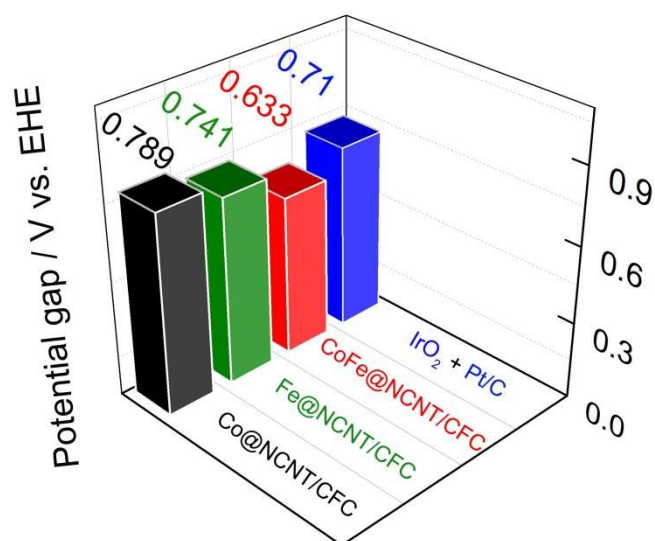


Figure S23. The overall oxygen performance ($\Delta E = E_{10} - E_{1/2}$) confirmed by half-wave potential for ORR and the potential for OER at $10 \text{ mA} \cdot \text{cm}^{-2}$.

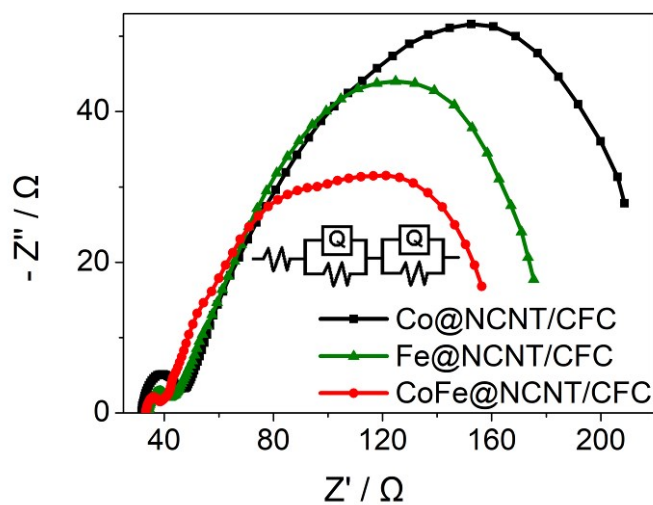


Figure S24. The Nyquist plots of Co@NCNT/CFC, Fe@NCNT/CFC and CoFe@NCNT/CFC for ORR at a potential of 0.87 V versus RHE, and the inset shows the corresponding equivalent circuit.

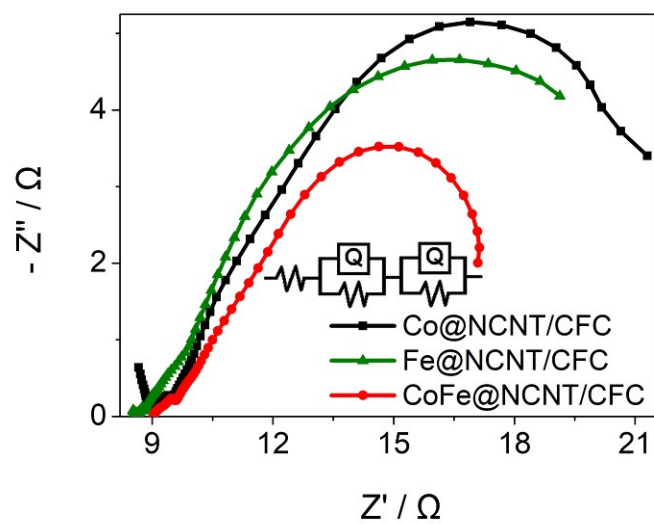


Figure S25. The Nyquist plots of Co@NCNT/CFC, Fe@NCNT/CFC and CoFe@NCNT/CFC for OER at a potential of 1.58 V versus RHE, and the inset shows the corresponding equivalent circuit.

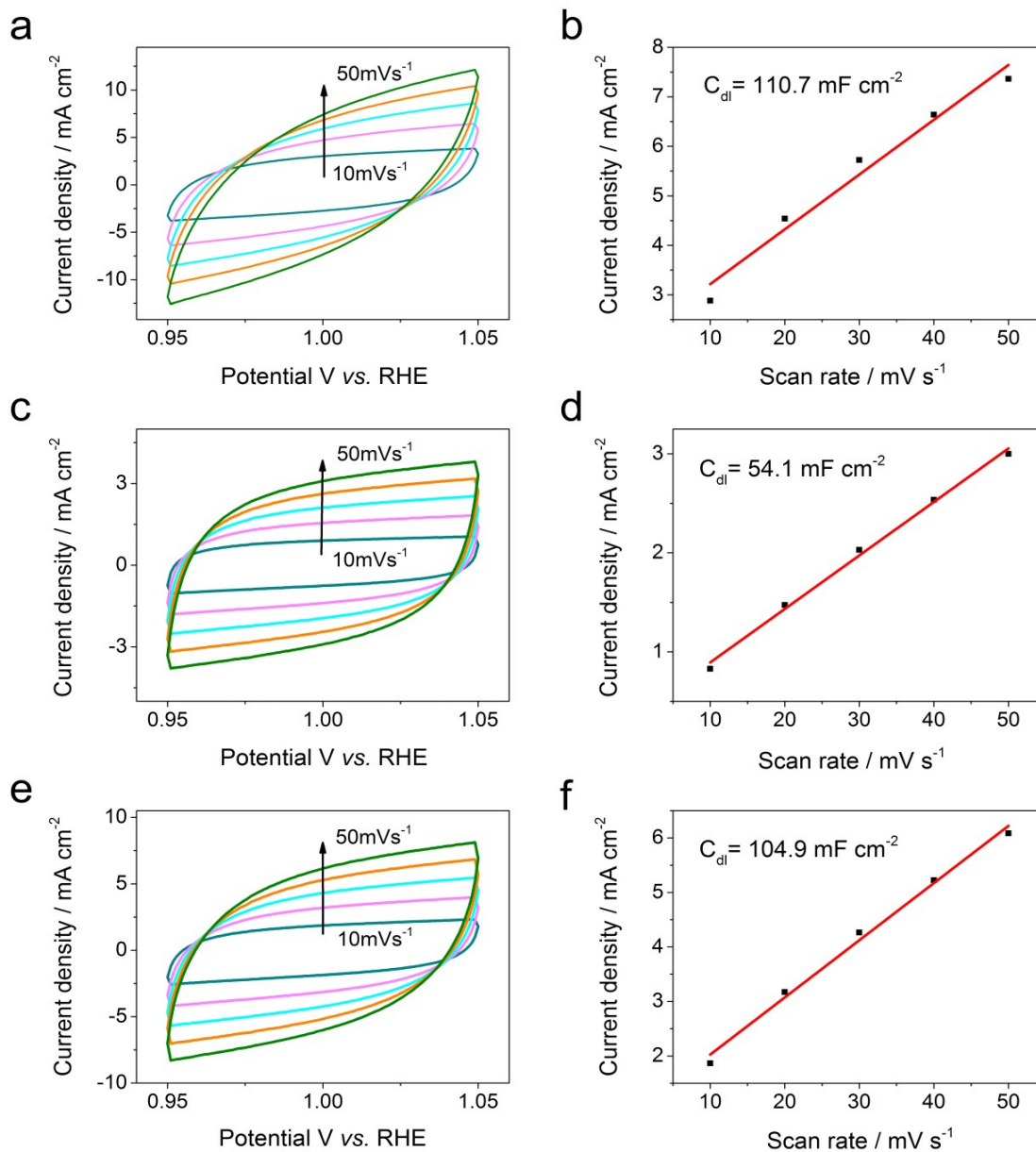


Figure S26. (a,c,e) The cyclic voltammograms curves of Co@NCNT/CFC, Fe@NCNT/CFC and CoFe@NCNT/CFC in the region of 0.95-1.05 V vs. RHE in 0.1 M KOH for OER. (b,d,f) The corresponding electrochemical double-layer capacitances of Co@NCNT/CFC, Fe@NCNT/CFC and CoFe@NCNT/CFC toward OER.

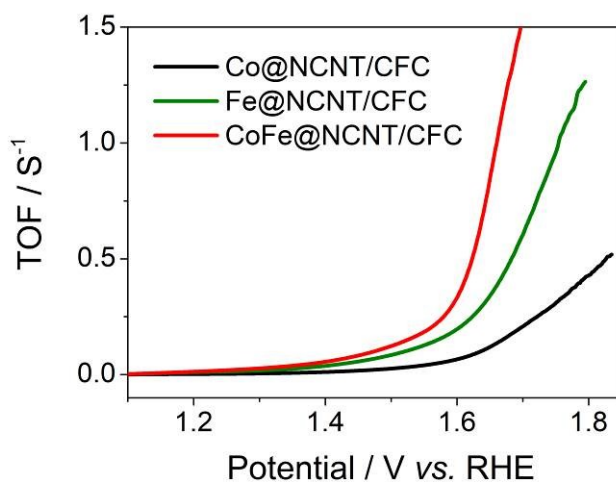


Figure S27. The calculated TOF data of Co@NCNT/CFC, Fe@NCNT/CFC and CoFe@NCNT/CFC for OER.

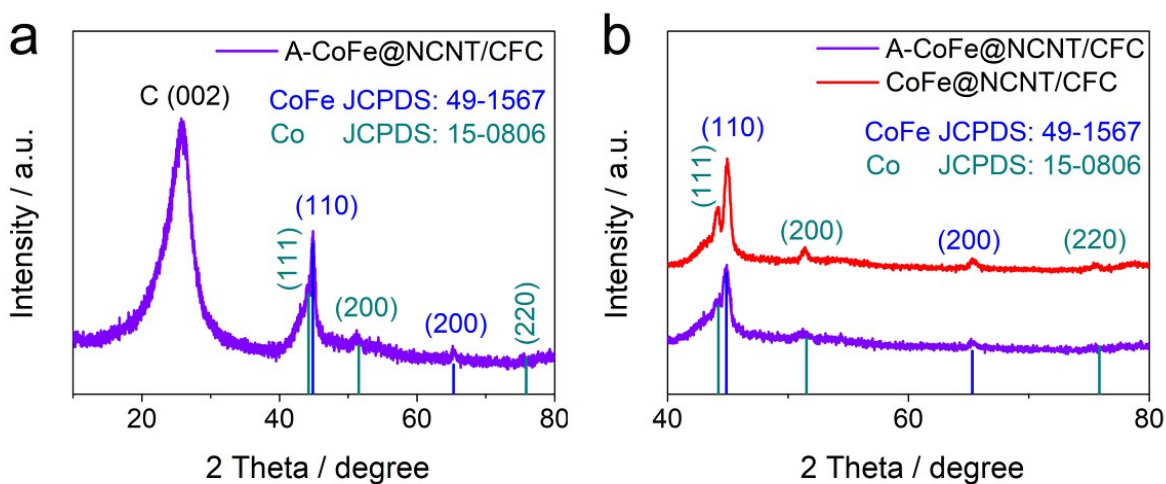


Figure S28. (a) The XRD pattern of A-CoFe@NCNT/CFC. (b) The magnification XRD patterns of CoFe@NCNT/CFC and A-CoFe@NCNT/CFC.

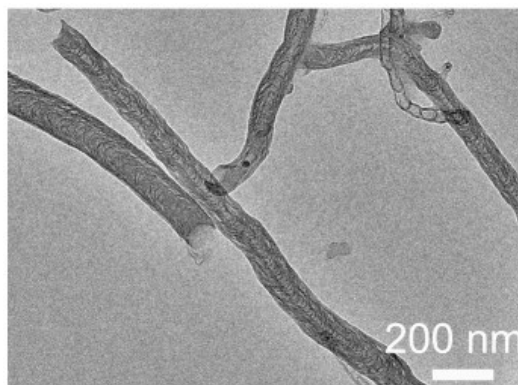


Figure S29. TEM of the A-CoFe@NCNT/CFC.

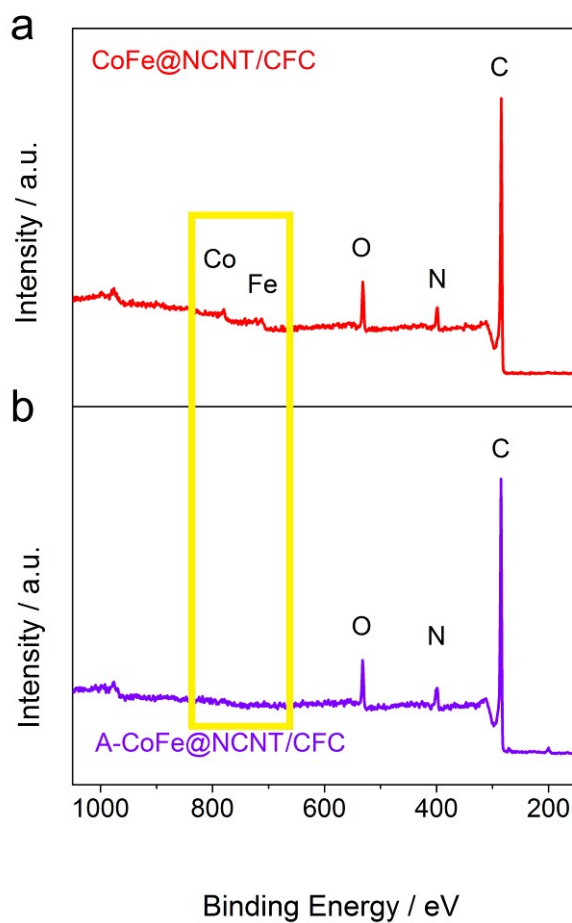


Figure S30. The XPS survey spectrum of (a) CoFe@NCNT/CFC and (b) A-CoFe@NCNT/CFC.

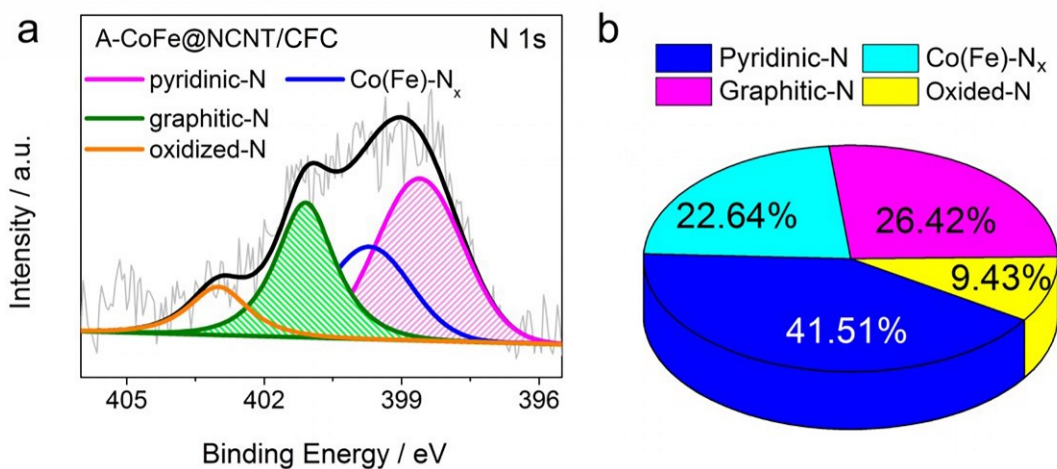


Figure S31. (a) N 1s XPS spectra of A-CoFe@NCNT/CFC and (b) the proportion of various N species of the N element in A-CoFe@NCNT/CFC.

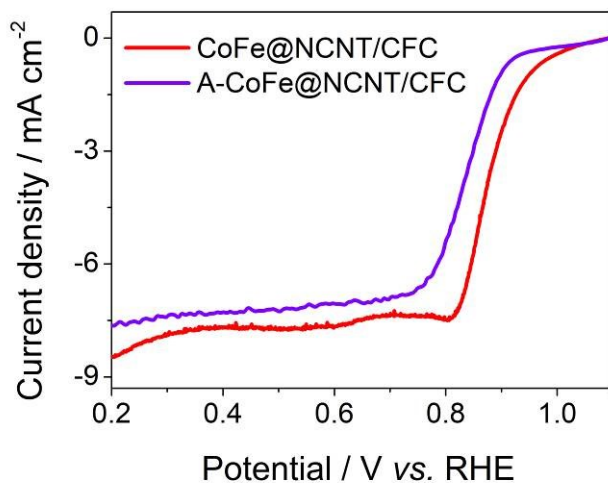


Figure S32. Polarization curves of CoFe@NCNT/CFC before and after acid treatment towards the ORR in 0.1 M KOH electrolyte.

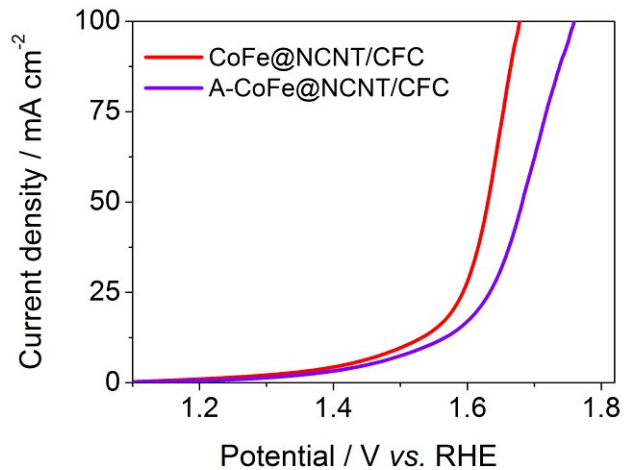


Figure S33. Polarization curves of CoFe@NCNT/CFC before and after acid treatment towards the OER in 0.1 M KOH electrolyte.

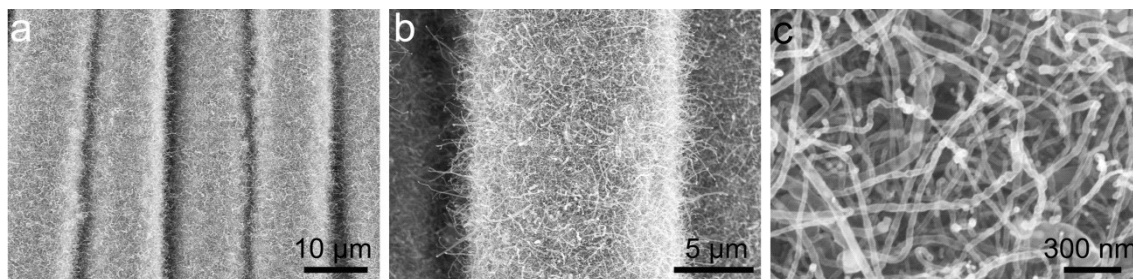


Figure S34. SEM images of CoFe@NCNT/CFC (ratio of Co to Fe is 2:1) carbonized at 700°C.

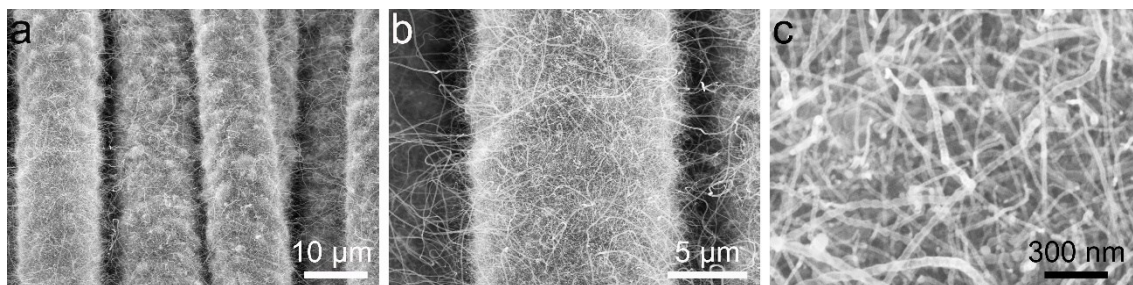


Figure S35. SEM images of CoFe@NCNT/CFC (ratio of Co to Fe is 2:1) carbonized at 900°C.

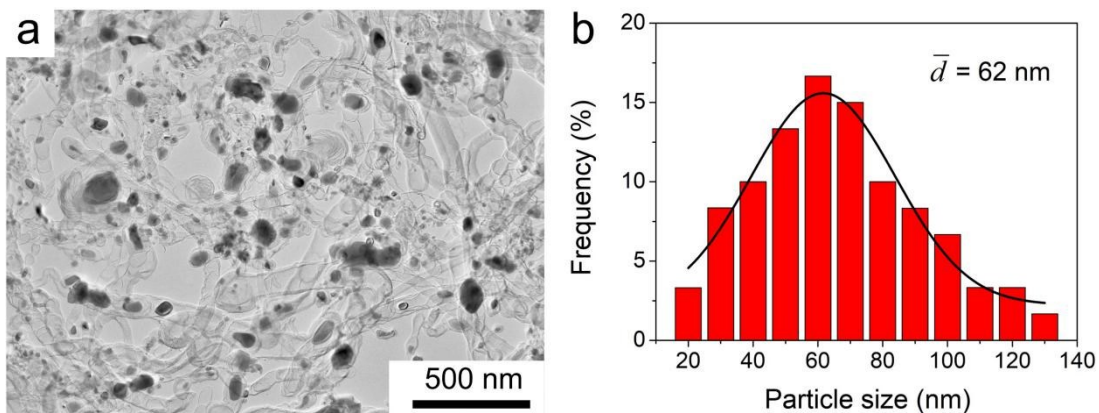


Figure S36. TEM images and particle size distribution diagram of CoFe@NCNT/CFC (ratio of Co to Fe is 2:1) carbonized at 700°C.

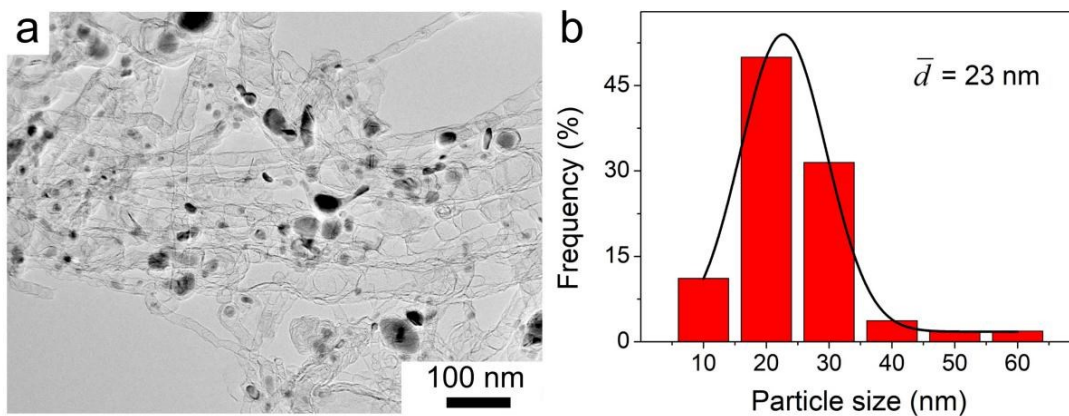


Figure S37. TEM images and particle size distribution diagram of CoFe@NCNT/CFC (ratio of Co to Fe is 2:1) carbonized at 900°C.

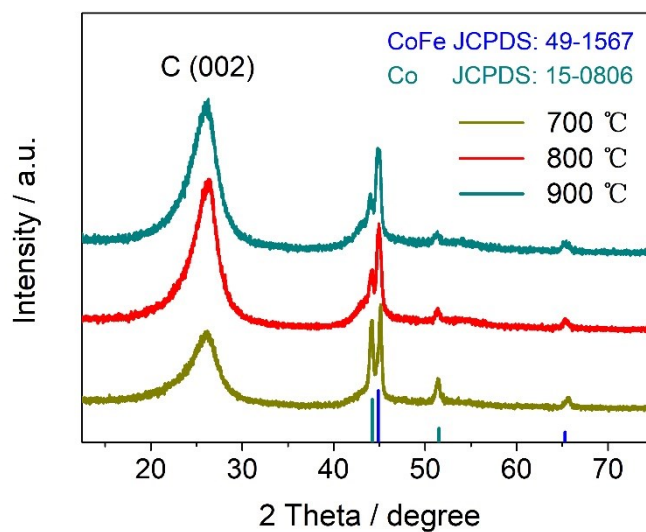


Figure S38. The XRD pattern of CoFe@NCNT/CFC (ratio of Co to Fe is 2:1) carbonized at 700°C, 800°C and 900°C.

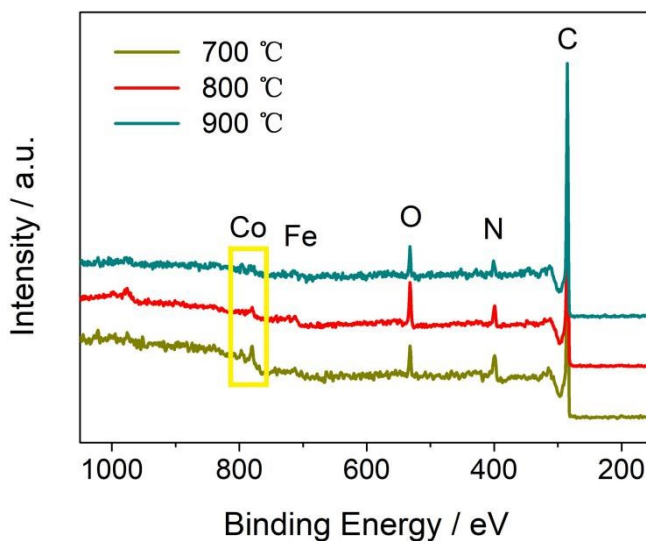


Figure S39. The XPS survey spectrum of CoFe@NCNT/CFC (ratio of Co to Fe is 2:1) carbonized at 700°C, 800°C and 900°C.

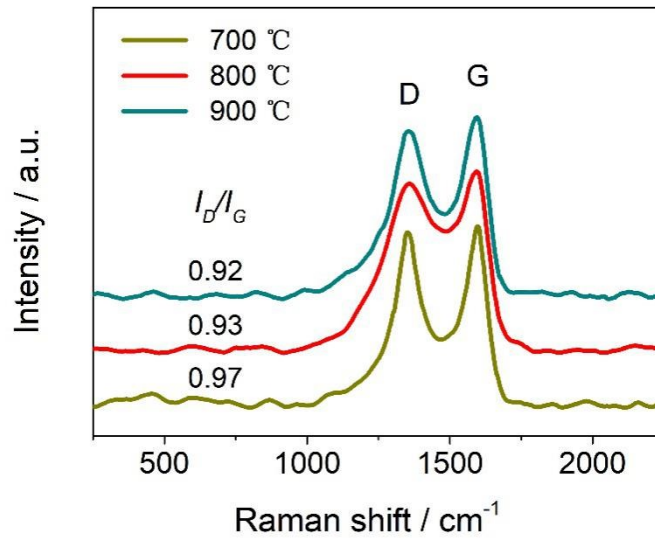


Figure S40. Raman spectra of CoFe@NCNT/CFC (ratio of Co to Fe is 2:1) carbonized at 700°C, 800°C and 900°C.

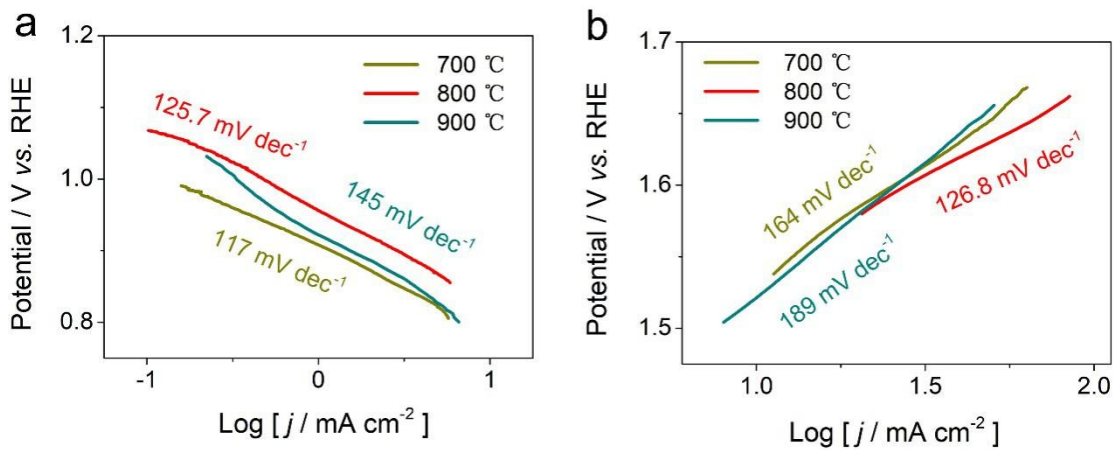


Figure S41. The Tafel plots of CoFe@NCNT/CFC (ratio of Co to Fe is 2:1) carbonized at 700°C, 800°C, 900°C for (a) ORR and (b) OER.

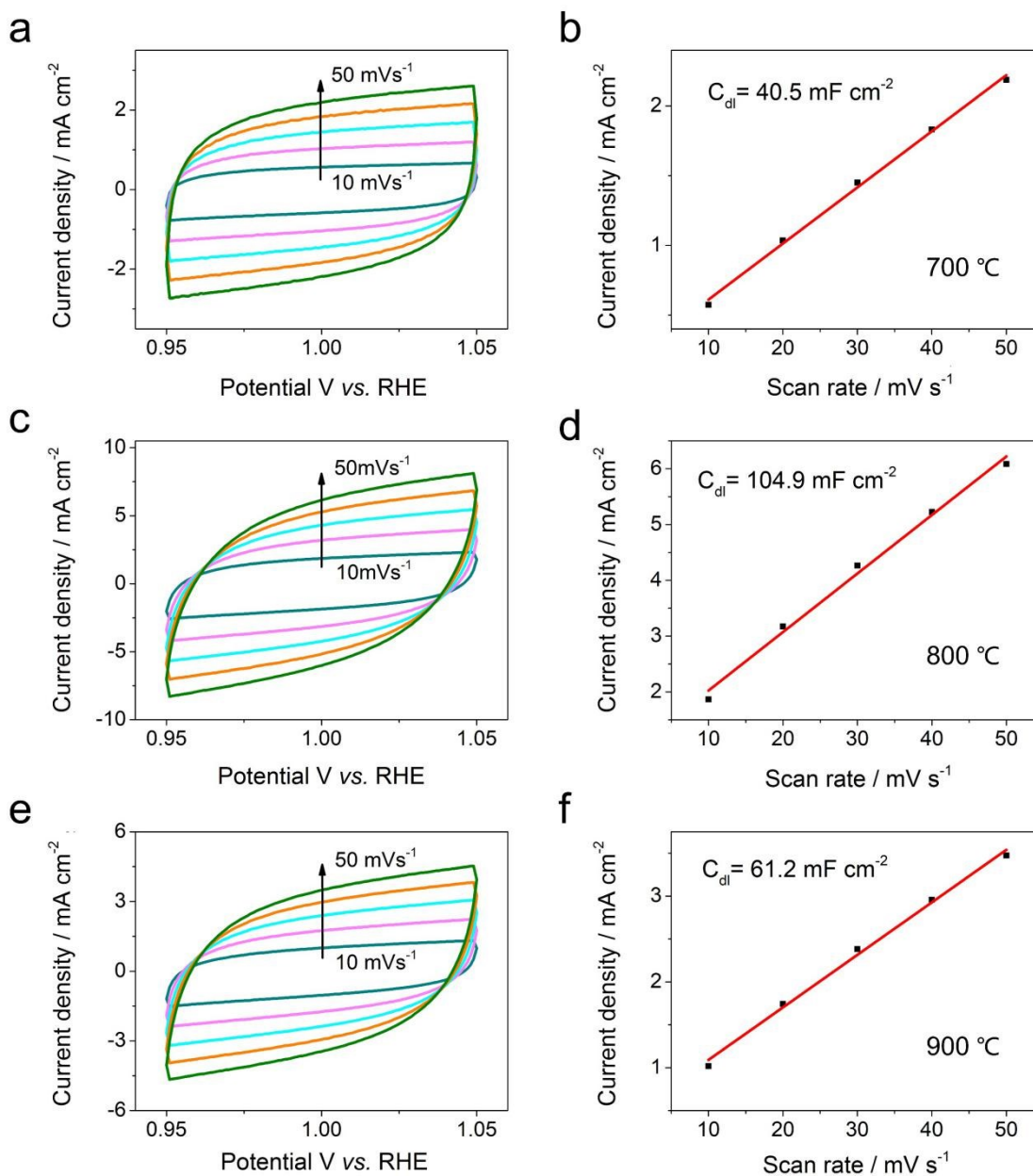


Figure S42. (a,c,e) The cyclic voltammograms curves of CoFe@NCNT/CFC (ratio of Co to Fe is 2:1, and carbonized at 700°C, 800°C and 900°C) in the region of 0.95-1.05 V vs. RHE in 0.1 M KOH for OER. (b,d,f) The corresponding electrochemical double-layer capacitances of CoFe@NCNT/CFC carbonized at 700°C, 800°C and 900°C toward OER.

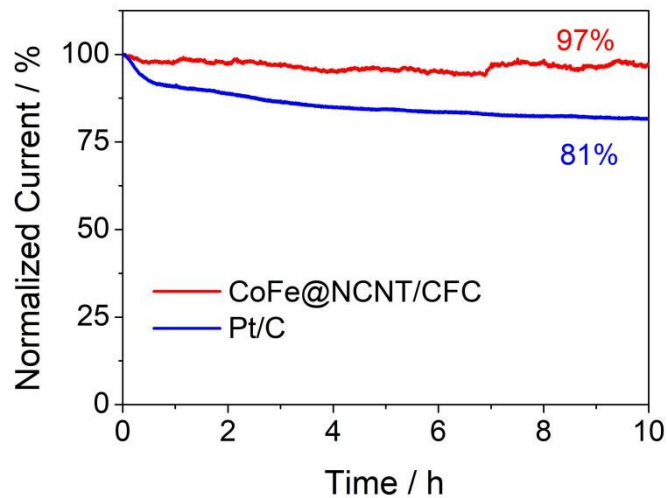


Figure S43. The Long-term stability of CoFe@NCNT/CFC and Pt/C for ORR at a potential of 0.4 V versus RHE.

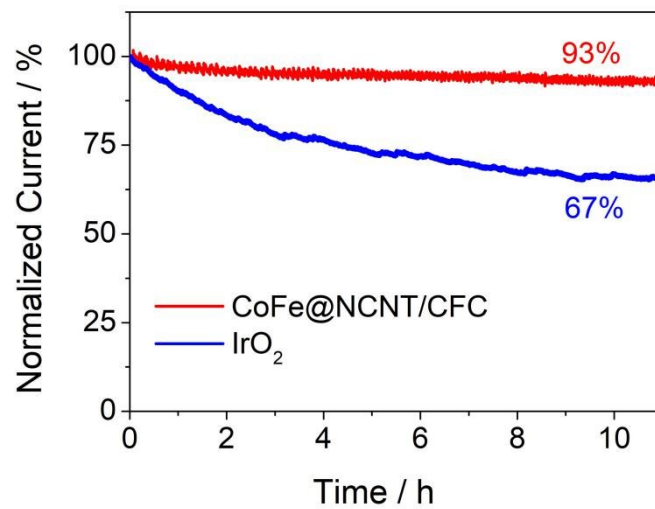


Figure S44. The Long-term stability of CoFe@NCNT/CFC and IrO₂ for OER at a potential of 1.53 V versus RHE.

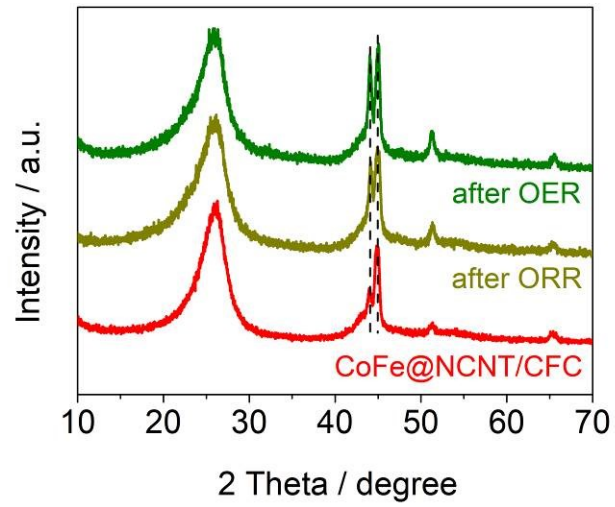


Figure S45. Comparison of XRD patterns of CoFe@NCNT/CFC before and after ORR and OER process.

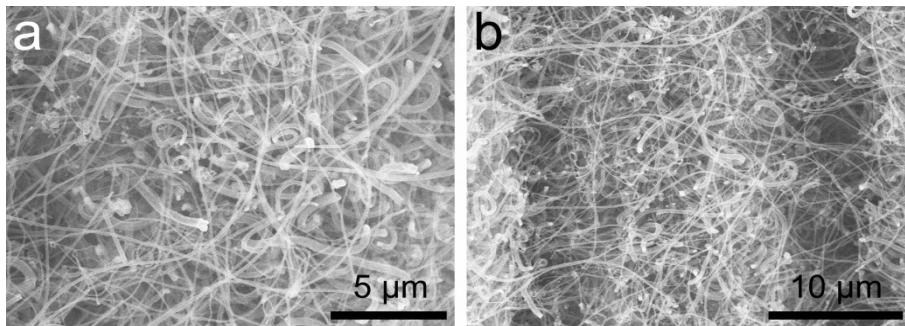


Figure S46. SEM images of the CoFe@NCNT/CFC after ORR process.

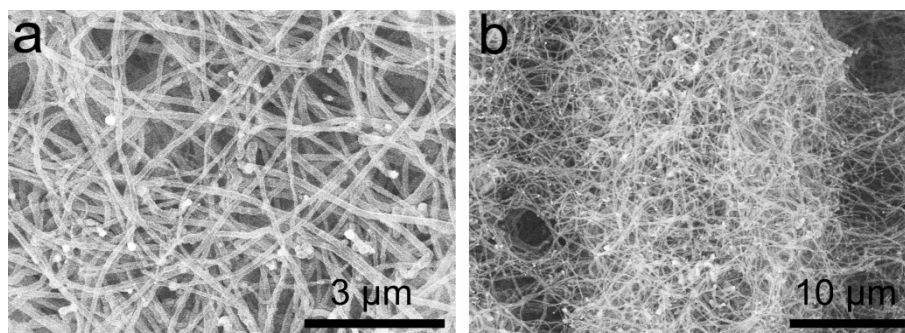


Figure S47. SEM images of the CoFe@NCNT/CFC after OER process.

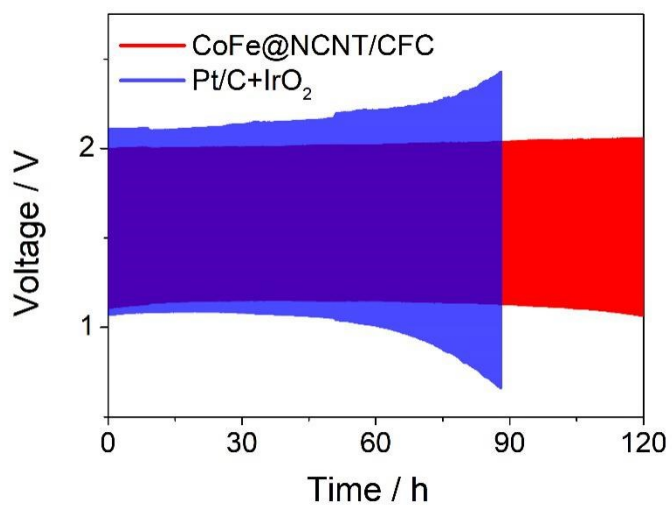


Figure S48. Galvanostatic discharge/charge cycling stability of the liquid ZABs with the CoFe@NCNT/CFC and Pt/C+IrO₂ air-cathodes at current density of 20 mA cm⁻².

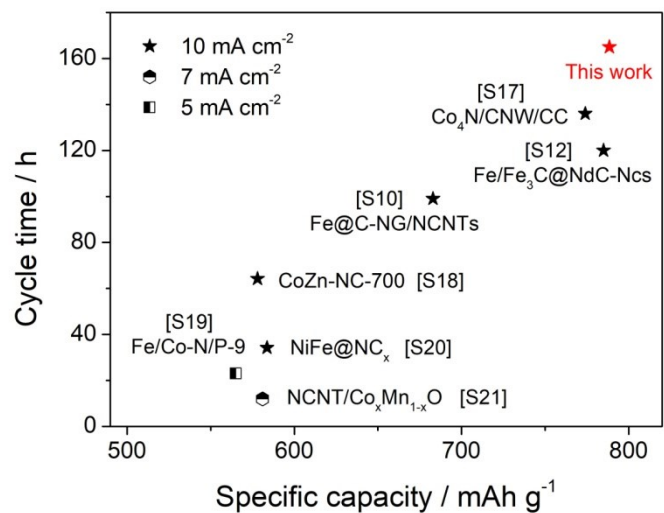


Figure S49. Comparison of the cycle life and specific capacity between CoFe@NCNT/CFC-based ZABs and some previously reported liquid rechargeable ZABs.

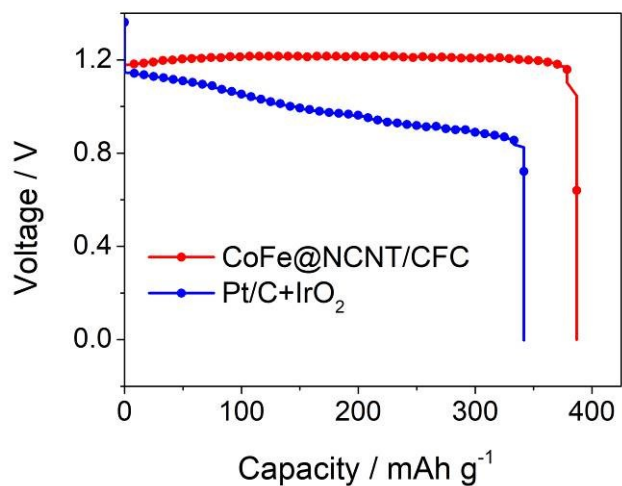


Figure S50. Specific capacity of the flexible all-solid-state rechargeable ZABs with CoFe@NCNT/CFC and commercial Pt/C+IrO₂ air cathodes at a discharge current density of 2 mA cm⁻².

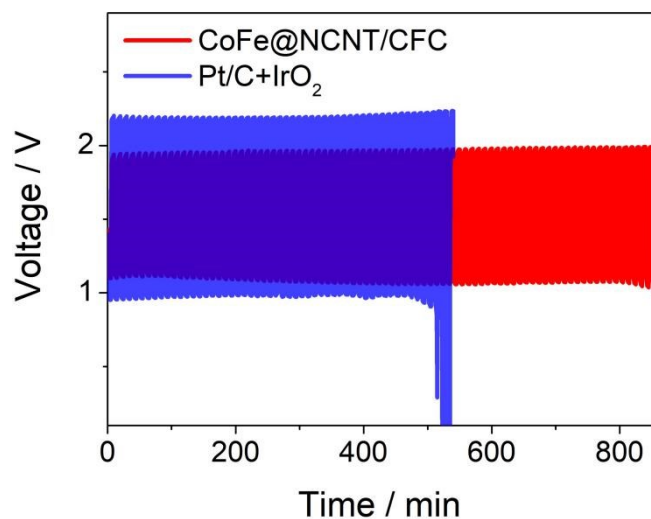


Figure S51. Galvanostatic discharge/charge cycling stability of the all-solid-state rechargeable ZABs by using CoFe@NCNT/CFC and Pt/C+IrO₂ as air-cathodes at 5 mA cm⁻².

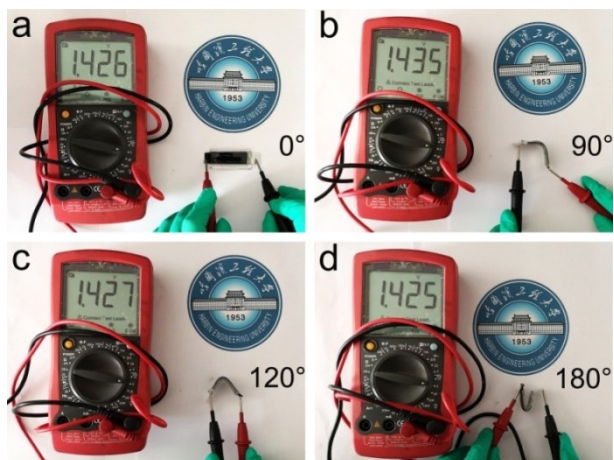


Figure S52. The open circuit of the flexible all-solid-state rechargeable ZABs with CoFe@NCNT/CFC air cathodes under different bending angles.

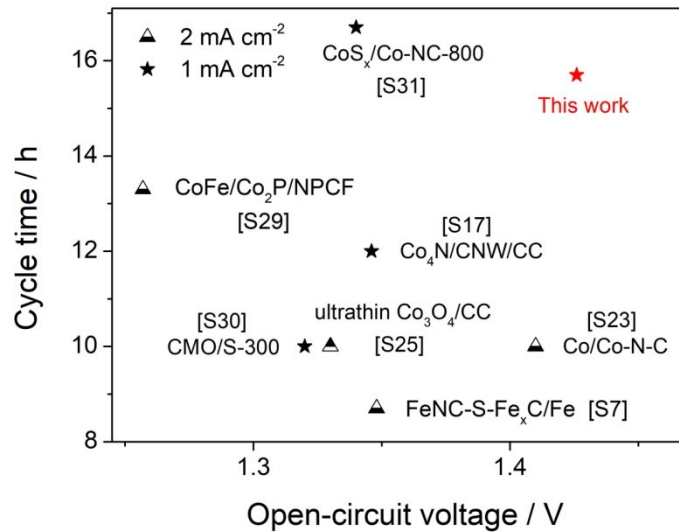


Figure S53. Comparison of the cycling life and open-circuit voltage between CoFe@NCNT/CFC-based ZABs and some previously reported solid ZABs.

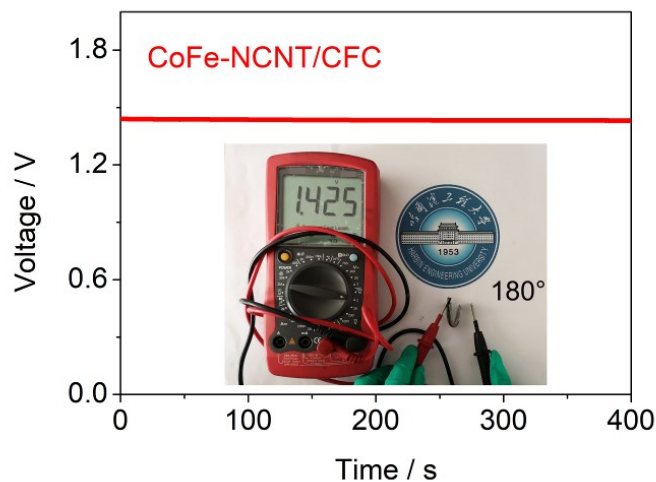


Figure S54. The open-circuit plots of one flexible all-solid-state ZABs based on CoFe@NCNT/CFC air cathodes with bending angles of 180°.

Table S1. The detailed diameter, length and mass loading of Co NWs / NCNT in the precursors/catalyst.

Precursors / Catalyst	Diameter of NWs/NRs or NCNT (nm)	Length of NWs/NRs or NCNT (μm)	Mass loading of NWs or NCNT
Co NWs/CFC	ca. 150 nm	ca. 10 μm	2.5 mg cm^{-2}
CoFe NWs/CFC	ca. 120 nm	ca. 5 μm	1.5 mg cm^{-2}
FeOOH NRs/CFC	ca. 70 nm	ca. 0.3 μm	1.5 mg cm^{-2}
Co@NCNT/CFC	ca. 145 nm	ca. 6 μm	2.0 mg cm^{-2}
CoFe@NCNT/CFC	ca. 122 nm	ca. 25 μm	1.2 mg cm^{-2}
Fe@NCNT/CFC	ca. 65 nm	ca. 4 μm	1.0 mg cm^{-2}

Table S2. The relative contents of various N species in the Co@NCNT/CFC, Fe@NCNT/CFC and CoFe@NCNT/CFC.

Catalyst	Pyridinic -N (at%)	M-N _x (at%)	Graphitic-N (at%)	Oxidized-N (at%)	Total (at%)
Co@NCNT/CFC	3.64	1.28 (Co-N _x)	3.58	0.96	9.46
Fe@NCNT/CFC	2.75	0.56 (Fe-N _x)	2.8	0.67	6.78
CoFe@NCNT/CFC	3.13	1.68(Co(Fe)-N _x)	2.02	0.56	7.39

Table S3. Comparison of electrocatalytic activity of our self-supported electrodes with recently reported highly active ORR/OER bifunctional oxygen electrode materials.

Catalyst	$E_{j=10}$ (V vs. RHE)	E_{onset} (V vs. RHE)	$E_{1/2}$ (V vs. RHE)	ΔE (V)	Ref.
Co@NCNT/CFC	1.603	0.96	0.814	0.789	This work
Fe@NCNT/CFC	1.565	0.91	0.824	0.741	This work
CoFe@NCNT/CFC	1.506	0.99	0.873	0.633	This work
Co ₂ P/CoN-in-NCNTs	1.65	0.96	0.85	0.80	S4
FeNi@NCNTs/CC	1.48	0.95	0.77	0.71	S6
FeNC-S-Fe _x C/Fe	1.553	1.05	0.873	0.68	S7
Co@N-CNTF-2	1.58	0.91	0.81	0.77	S8
N-GCNT/FeCo	1.73	1.03	0.92	0.81	S9
Fe@C-NG/NCNTs	1.68	0.93	0.84	0.84	S10
Co-N-CNTs	1.69	0.97	0.90	0.79	S11
Fe/Fe ₃ C@NdC-NCs	1.62	0.92	0.83	0.79	S12
Fe ₃ C/Co(Fe)O _x @NCNT	1.58	—	0.86	0.72	S13
S,N-Fe/N/C-CNT	1.60	—	0.85	0.75	S14
FeCo/FeCoNi@NCNTs-HF	1.608	—	0.85	0.758	S15
CoFe/N-GCT	1.67	0.91	0.79	0.88	S16

Table S4. Comparison of the liquid rechargeable ZABs performance of CoFe@NCNT/CFC with various bifunctional catalysts in the recent literatures.

Catalyst	Specific capacity (mA cm ⁻² , mAh g ⁻¹)	Recharge-ability (min/cycle, cycle number, time)	Ref.
CoFe@NCNT/CFC	788.5 (10 mA/cm ⁻²)	10 min /cycle for 990 cycles (165h)	This work
Co ₂ P/CoN-in-NCNTs	649.6 (20 mA/cm ⁻²)	60 min /cycles for 96 h (5 mA/cm ⁻²)	S4
Co ₄ N/CNW/CC	774 (10 mA/cm ⁻²)	20 min /cycle for 408 cycles (136 h)	S17
CoZn-NC-700	578 (10 mA/cm ⁻²)	10 min /cycle for 385 cycles (64.2 h)	S18
Fe@C-NG/NCNTs	683 (10 mA/cm ⁻²)	20 min /cycle for 297 cycles (99 h)	S10
Fe/Co-N/P-9	565 (5 mA/cm ⁻²)	10 min /cycle for ≈23h	S19
NiFe@NC _x	583.7 (10 mA/cm ⁻²)	10 min /cycle for 205 cycles (34.2 h)	S20
Fe/Fe ₃ C@NdC-NCs	785 (10 mA/cm ⁻²)	20 min /cycle for 360 cycles (120 h)	S12
Fe ₃ C/Co(Fe)O _x @NCNT	—	10 min /cycle for 150 cycles (25 h)	S13
NCNT/Co _x Mn _{1-x} O	581 (7 mA/cm ⁻²)	10 min /cycle for 12 h	S21
NiCo ₂ O ₄ @N-OCNT	—	800 s / cycle for 190 cycles (≈42.2 h)	S22

Table S5. Comparison of the flexible all-solid rechargeable ZABs performance of CoFe@NCNT/CFC with various bifunctional catalysts in the recent literature.

Catalyst	OCV (V)	Power density (mW cm ⁻²)	Recharge-ability (min/cycle, cycle number, time)	Ref.
CoFe@NCNT/CFC	1.426	37.7	10 min/cycle for 94 cycles(15.7 h)	This work
Co/Co-N-C	1.41	—	10 min/cycle for 10 h (2 mA cm ⁻²)	S23
Silk NC/KB		32.3	10 min/cycle for 30 cycles (5 h)	S24
ultrathin Co ₃ O ₄ /CC	1.33	—	20 min/cycle for 10 h (2 mA cm ⁻²)	S25
FeNC-S-Fe _x C/Fe	1.348	—	≈ 8.7 h (2 mA cm ⁻²)	S7
N-GQDs/NiCo ₂ S ₄ /CC	1.406	26.2	—	S26
Co ₄ N/CNW/CC	1.346	—	20 min /cycle for 36 cycles (12 h)	S17
N, S-CC	1.247	47 (mW cm ⁻³)	4 min /cycle for 8 h (5 mA cm ⁻³)	S27
Co-N-CNTs	1.365	—	—	S11
P-CoSe ₂ /N-C	1.3	≈ 23	20 min /cycle for 55 cycles (18.3h)	S28
FeCo/Co ₂ P@NPCF	1.257		10 min/cycle for 13.3 h (2 mA cm ⁻²)	S29
CMO/S-300	1.32		30 min /cycle for 20 cycles (10 h)	S30
CoS _x /Co-NC-800	1.34		10 min/cycle for 100 cycles(16.7 h)	S31

REFERENCES

- S1 J. Q. Tian, Q. Liu, A. M. Asiri and X. P. Sun, *J. Am. Chem. Soc.*, 2014, **136**, 7587-7590.
- S2 H. F. Liang, C. Xia, A.-H. Emwas, D. H. Anjum, X. H. Miao and H. N. Alshareef, *Nano Energy*, 2018, **49**, 155-162.
- S3 Y. H. Han, Y. G. Wang, R. R. Xu, W. X. Chen, L. R. Zheng, A. J. Han, Y. Q. Zhu, J. Zhang, H. B. Zhang, J. Luo, C. Chen, Q. Peng, D. S. Wang and Y. D. Li, *Energy Environ. Sci.*, 2018, **11**, 2348-2352.
- S4 Y. Y. Guo, P. F. Yuan, J. N. Zhang, H. C. Xia, F. Y. Cheng, M. F. Zhou, J. Li, Y. Y. Qiao, S. C. Mu and Q. Xu, *Adv. Funct. Mater.*, 2018, **28**, 1805641.
- S5 T. F. Jaramillo, K. P. Jorgensen, J. Bonde, J. H. Nielsen, S. Horch and I. Chorkendorff, *Science*, 2007, **317**, 100-102.
- S6 X. T. Zhao, S. C. Abbas, Y. Y. Huang, J. Q. Lv, M. X. Wu and Y. B. Wang, *Adv. Mater. Interface.*, 2018, **5**, 1701448.
- S7 Y. Y. Qiao, P. F. Yuan, Y. F. Hu, J. N. Zhang, S. C. Mu, J. H. Zhou, H. Li, H. C. Xia, J. He and Q. Xu, *Adv. Mater.*, 2018, **30**, 1804504.
- S8 H. L. Guo, Q. C. Feng, J. X. Zhu, J. S. Xu, Q. Q. Li, S. L. Liu, K. W. Xu, C. Zhang and T. X. Liu, *J. Mater. Chem. A*, 2019, **7**, 3664-3672.
- S9 C. Y. Su, H. Cheng, W. Li, Z. Q. Liu, N. Li, Z. F. Hou, F. Q. Bai, H. X. Zhang and T. Y. Ma, *Adv. Energy Mater.*, 2017, **7**, 1602420.
- S10 Q. C. Wang, Y. P. Lei, Z. Y. Chen, N. Wu, Y. B. Wang, B. Wang and Y. D. Wang, *J. Mater. Chem. A*, 2018, **6**, 516-526.

- S11 T. T. Wang, Z. K. Kou, S. C. Mu, J. P. Liu, D. P. He, I. S. Amiin, W. Meng, K. Zhou, Z. X. Luo, S. Chaemchuen and F. Verpoort, *Adv. Funct. Mater.*, 2018, **28**, 1705048.
- S12 Z. Q. Cao, H. B. Hu, M. Z. Wu, K. Tang and T. T. Jiang, *J. Mater. Chem. A*, 2019, **7**, 17581-17593.
- S13 M. F. Wang, T. Qian, S. S. Liu, J. Q. Zhou and C. L. Yan, *ACS Appl. Mater. Interfaces.*, 2017, **9**, 21216-21224.
- S14 P. Z. Chen, T. P. Zhou, L. L. Xing, K. Xu, Y. Tong, H. Xie, L. D. Zhang, W. S. Yan, W. S. Chu, C. Z. Wu and Y. Xie, *Angew. Chem., Int. Ed.*, 2017, **56**, 610-614.
- S15 Z. Wang, J. M. Ang, B. W. Zhang, Y. F. Zhang, X. Y. D. Ma, T. Yan, J. Liu, B. Y. Che, Y. Z. Huang and X. H. Lu, *Applied Catalysis B: Environmental*, 2019, **254**, 26-36.
- S16 X. Liu, L. Wang, P. Yu, C. G. Tian, F. F. Sun, J. Y. Ma, W. Li and H. G. Fu, *Angew. Chem., Int. Ed.*, 2018, **57**, 16166-16170.
- S17 F. L. Meng, H. X. Zhong, D. Bao, J. M. Yan and X. B. Zhang, *J. Am. Chem. Soc.*, 2016, **138**, 10226-10231.
- S18 B. H. Chen, X. B. He, F. X. Yin, H. Wang, D.-J. Liu, R. X. Shi, J. N. Chen and H. W. Yin, *Adv. Funct. Mater.*, 2017, **27**, 1700795.
- S19 J. Di, J. X. Guo, N. N. Wang and G. P. Ma, *ACS Sustainable Chem. Eng.*, 2019, **7**, 7716-7727.
- S20 J. B. Zhu, M. L. Xiao, Y. L. Zhang, Z. Jin, Z. Q. Peng, C. P. Liu, S. L. Chen, J. J. Ge and W. Xing, *ACS Catal.*, 2016, **6**, 6335-6342.
- S21 X. Liu, M. Park, M. G. Kim, S. Gupta, X. J. Wang, G. Wu and J. Cho, *Nano Energy*, 2016,

20, 315-325.

S22 S. Zeng, X. Tong, S. S. Zhou, B. Lv, J. Qiao, Y. H. Song, M. H. Chen, J. T. Di and Q. W. Li, *Small*, 2018, **14**, 1803409.

S23 P. Yu, L. Wang, F. F. Sun, Y. Xie, X. Liu, J. Y. Ma, X. W. Wang, C. G. Tian, J. H. Li and H. G. Fu, *Adv. Mater.*, 2019, **31**, 1901666.

S24 C. Y. Wang, N.-H. Xie, Y. L. Zhang, Z. H. Huang, K. L. Xia, H. M. Wang, S. J. Guo, B.-Q. Xu and Y. Y. Zhang, *Chem. Mater.*, 2019, **31**, 1023-1029.

S25 X. Chen, B. Liu, C. Zhong, Z. Liu, J. Liu, L. Ma, Y. D. Deng, X. P. Han, T. P. Wu, W. B. Hu and, J. Lu, *Adv. Energy Mater.*, 2017, **7**, 1700779.

S26 W. W. Liu, B. H. Ren, W. Y. Zhang, M. W. Zhang, G. R. Li, M. L. Xiao, J. B. Zhu, A. P. Yu, L. Ricardez-Sandoval and Z. W. Chen, *Small*, 2019, **15**, 1903610.

S27 Z. Zhao, Z. K. Yuan, Z. S. Fang, J. H. Jian, J. Li, M. J. Yang, C. S. Mo, Y. Zhang, X. H. Hu, P. Li, S. Y. Wang, W. Hong, Z. K. Zheng, G. F. Ouyang, X. D. Chen and D. S. Yu, *Adv. Sci.*, 2018, **5**, 1800760.

S28 H. Zhang, T. T. Wang, A. Sumboja, W. J. Zang, J. P. Xie, D. Q. Gao, S. J. Pennycook, Z. L. Liu, C. Guan and J. Wang, *Adv. Funct. Mater.*, 2018, **28**, 1804846.

S29 Q. Shi, Q. Liu, Y. Ma, Z. Fang, Z. Liang, G. Shao, B. Tang, W. Y. Yang, L. Qin and X. S. Fang, *Adv. Energy Mater.* 2020, **10**, 1903854.

S30 S. J. Peng, X. P. Han, L. L. Li, S. L. Chou, D. X. Ji, H. J. Huang, Y. H. Du, J. Liu and S. Ramakrishna, *Adv. Energy Mater.*, 2018, **8**, 1800612.

S31 Q. Lu, J. Yu, X. H. Zou, K. M. Liao, P. Tan, W. Zhou, M. Ni and Z. P. Shao, *Adv. Funct.*

Mater. 2019, **29**, 1904481.